Reports

A Tunnel in the Large Ribosomal Subunit Revealed by Three-Dimensional Image Reconstruction

A. YONATH, K. R. LEONARD, H. G. WITTMANN

A better understanding of the molecular mechanism of protein biosynthesis depends on the availability of a reliable model for the ribosome particle. The application of a diffraction technique, namely, three-dimensional image reconstruction from two-dimensional sheets of the large ribosomal subunits of *Bacillus stearothermophilus* at a resolution of 30 angstroms is described. The resulting three-dimensional model shows at least four projecting arms, arranged radially near the presumed interface with the 30S subunit. The projecting arms are positioned around a cleft, which turns into a tunnel with a length of 100 to 120 angstroms and a diameter of up to 25 angstroms. This tunnel spans the particle and may provide the path taken by the nascent polypeptide chain.

TO BETTER UNDERSTAND THE ROLE of ribosomes in protein biosynthesis, we have initiated structural studies of these particles by diffraction methods, and we have developed an in vitro crystallization procedure for intact ribosomal particles from bacterial sources. Three-dimensional crystals of 70S ribosomes from *Escherichia coli* (*1*) and of the large ribosomal subunits from *Halobacterium marismortui* (*2, 3*) and *Bacillus stearothermophilus* (*4–6*) diffracting x-rays to 6 and 13 Å, respectively, were obtained. From the latter species we were able to grow two types of well-ordered two-dimensional crystalline sheets: AL using alcohols (*7*) and ST using salt mixtures (*6–8*). These sheets are suitable for studies by image reconstruction.

Structure determination by three-dimensional image reconstruction from two-dimensional sheets is justified not only because it may yield significant results, but also because of its expected contribution to subsequent x-ray crystallographic analysis. A model obtained from image reconstruction may be used for gradual phasing of low-resolution crystallographic data. These phases, in turn, may help locate heavy atom sites for the isomorphous replacement technique.

Both AL and ST two-dimensional sheets consisted of small unit cells: 145 ± 3 × 311 ± 14 Å, $\gamma = 89° \pm 2.6°$ for the arrays grown in alcohol, and 148 ± 10 × 370 ± 20 Å, $\gamma = 109° \pm 3°$ for those grown from salts. These cell dimensions are close to those of forms 1 and 2 of our three-dimensional crystals (*6, 9*). The AL and ST sheets were well ordered, and optical diffraction patterns of electron micrographs of negatively stained specimens extended to 30 and 28 Å, respectively (Fig. 1). In both cases each unit cell contained two particles with dimensions similar to those obtained by other methods (*10*).

Because only a small fraction of the particles in the drop actually constitute the two-dimensional sheets, we could not separate them from the rest of the drop. Therefore, we tested the migration profile on sucrose gradients and the biological activity of the ribosomal particles in the crystallizing drops in the poly-U system (*11*). Particles subjected to crystallization conditions comigrated with standard particles and maintained their biological activity.

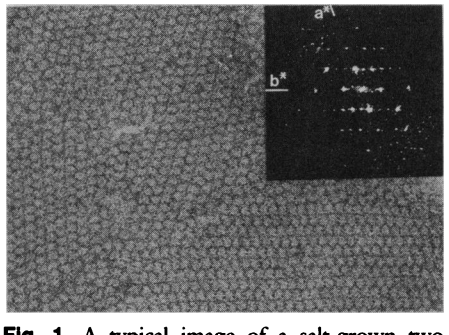

Fig. 1. A typical image of a salt-grown two-dimensional sheet stained by gold-thioglucose, and an optical diffraction pattern from a single crystalline domain containing about 20 × 10 unit cells. The a* and b* axes have been labeled. Areas for three-dimensional image reconstruction were chosen by using their optical diffractions according to the following criteria: (i) best resolution, (ii) patterns with sharpest reflections in patterns with no spurious spots, that is, including only one lattice region with the minimum mosaic spread. Only the strongest diffraction spots are shown. The others, although weak, contributed significantly to the resulting model, as shown in Fig. 5. Two-dimensional sheets were prepared as described (*7, 8*). Crystallization mixtures (7 to 10 μl) were applied to the plastic side of carbon-coated nitrocellulose grids and stained for 10 seconds with 1% (w/v) gold-thioglucose. Excess liquid was then removed by blotting. The grids were examined with a 400T Phillips electron microscope (operating at 80 kV) at an electron optical magnification of ×28,000.

We have used AL and ST sheets from three different preparations of ribosomes. We negatively stained them with either gold-thioglucose or uranyl acetate. Unlike uranyl acetate, which may interact chemically with the negatively charged components of the ribosomal particles [most likely the ribosomal RNA (rRNA)], gold-thioglucose is an inert stain that is expected to reveal the outer contour of the particles.

We have performed seven reconstructions, processed about 250 micrographs, and investigated 13 independently reconstructed particles. For each reconstruction we have used between two and four complete tilt series obtained from two-dimensional sheets. Two of these tilt series were perpendicular to each other. Between 20 and 25 crystallographically independent lattice lines, extending to a maximum resolution of 28 Å, were extracted for each reconstruction (Fig. 2).

We present here a three-dimensional model at 30 Å resolution (Fig. 3) reconstructed from three tilt series of crystalline sheets grown from salts and negatively stained with gold-thioglucose. This model is compared with those reconstructed from sheets stained with uranyl acetate.

The particles within the cells of the AL sheets were related by $p12_1$ symmetry (*7*). Although it appears that the ST sheets (Fig. 1) also contained crystallographic dimers, this was true only at lower resolution (45 Å). Three-dimensional image reconstructions were therefore carried out under the assumption of $p12_1$ symmetry for the AL crystals and p1 symmetry for the ST ones. In all reconstructions, the two particles in the unit cell showed the same essential features. However, in those reconstructed with p1 symmetry, generally one particle in the unit cell was resolved better than the other. This result may stem from preferential staining or differences in preservation.

The reconstructed particle (Fig. 3) has dimensions similar to those determined by other physical methods (*10*), and its volume (1.8×10^6 Å^3) corresponds to about 90% of the whole particle. On the basis of the known molecular weight of this particle (1.6×10^6) and of the volume obtained from the three-dimensional image reconstruction, the calculated density of a 50S particle is 1.3 to 1.4 g/cm^3, and the molecu-

A. Yonath, Weizmann Institute of Science, Rehovot, Israel, and Max Planck Research Unit for Structural Molecular Biology, 2000 Hamburg 52, FRG.
K. R. Leonard, European Molecular Biology Laboratory, 6900 Heidelberg, FRG.
H. G. Wittmann, Max-Planck-Institut für Molekulare Genetik, 1000 Berlin, FRG.

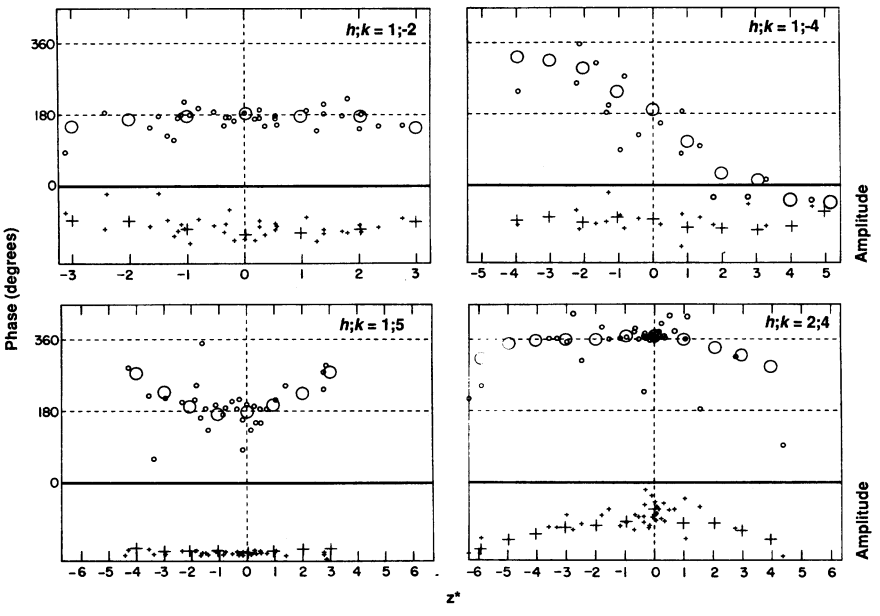

Fig. 2. Variation of phases along four typical lattice lines from which the three-dimensional model was synthesized. All amplitudes were adjusted to the same maximum value. Small circles represent the experimental values of the phases obtained by computer processing of the images, and the large ones are the interpolated values. z^* is the distance from the midpoint of the lattice line. Images were recorded at a dose of 10 electrons per square angstrom, of the specimens tilted at angles up to 55°, at intervals of 5°, with respect to the incident electron beam. A typical tilt series contained 23 images of which the first, middle, and last images were untilted. This control was essential for establishing that the specimen was not severely damaged by the electron beam during recording of the tilt series. No differences have been detected among the diffraction patterns of the untilted views taken at all stages of the experiment. The images were analyzed by standard methods (*22*) as described previously (*23*). All computational steps were carried out on a VAX 11/780. Ordered areas in the images were selected by optical diffraction and scanned with a microdensitometer (Optronics-1000) with a 25-μm raster, corresponding to 9 Å at the specimen. For Fourier transforms, optical densities of arrays (512 × 512) were used, and reciprocal lattices were fitted to the calculated diffraction patterns. Amplitudes and phases were extracted from peaks of at least 2 SD above background. Images of untilted sheets were used for the initial data in the three-dimensional analysis. The data were combined with a comparison range in z^* of 0.0016 $Å^{-1}$. The average phase error for each image based on a cumulative comparison of individual phases was 20° to 30°. Each lattice line was sampled at regular intervals of 1/300 $Å^{-1}$ along smooth curves fitted manually to the experimental values to provide terms for the Fourier synthesis. Terms along the 0,0 lattice line were not included. Fourier synthesis of 130 to 300 terms yielded the three-dimensional maps.

lar volume (V_m) for a hypothetical crystal of a thickness of the sheets (160 to 170 Å) is 2.6 to 2.7 $Å^3$ per dalton. Both values are in good agreement with values tabulated by Matthews (*12*) and calculated for other large nucleoprotein structures (*13, 14*).

Several features were revealed by our analysis (Fig. 3). The concave surface of the particle consisted of several protrusions 25 to 30 Å in diameter. A long arm was located on the other side of the particle (bottom of the particle shown in Fig. 3A). Several projecting arms, two of which were longer than the others, were arranged radially around the edge (upper side of the particle shown in Fig. 3A). A narrow elongated cleft was formed between the projecting arms and turned into a tunnel up to 25 Å in diameter and 100 to 120 Å long (Fig. 3, B–D).

The tunnel was present in all reconstructions of the *ST* sheets independent of the staining material. Furthermore, indications of such a tunnel were detected in some filtered images of particular tilts (Fig. 4). In

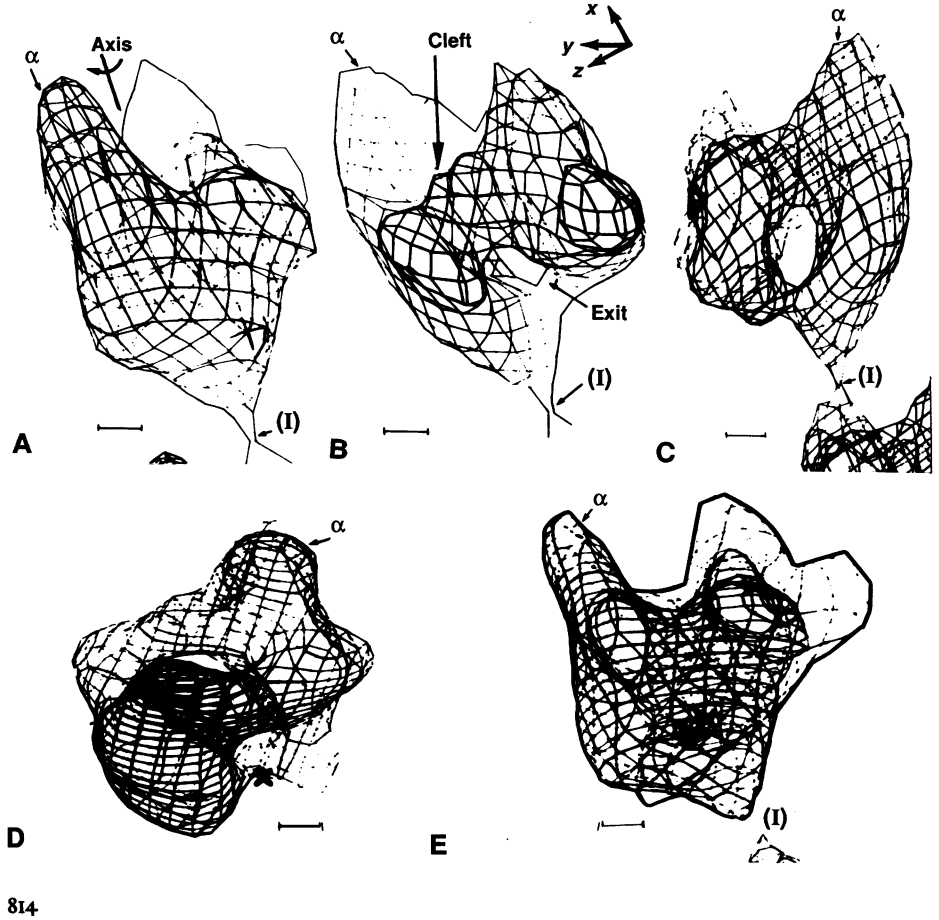

Fig. 3. Computer graphic display of the outline of the reconstructed model of the 50*S* ribosomal subunit at 30 Å resolution. The front is contoured with heavy lines, the back with lighter ones. Bar length, 20 Å. The asterisk marks the exit from the tunnel on the other side of the ribosome. Alpha (α) marks the longest projecting arm. The contour level for the particle boundary was chosen to be that at which the interparticle contacts could be resolved. For real-time display we used the computer program FRODO (*24*) combined with the GHC650 (written by G. H. Cohen, NIH) for Fourier synthesis, and FRODOMAP (written by J. L. Bhat, NIH) as well as the version, written by H. Bosshard, EMBL, Heidelberg. Views (A) to (C) were obtained from one reconstruction, and views (D) and (E) from another. (**A**) A side view of the model. The entire particle and part of a second one are shown. The arrow (I) points at the crystal contact between the two particles. (**B**) The model in (A) was rotated about the axis shown to generate the model in (B). (**C**) The model shown in (A and B) viewed into the branch of the tunnel from the exit point. (**D**) A view into the tunnel from the cleft. (**E**) The model viewed in a projection that resembles models derived from electron microscopy of single particles. The contour level is 2 to 5% higher than in previous views.

every reconstructed particle there was also a region of low density that branched off the tunnel at an angle of 60° to 70° to form a Y (or V) shape and terminated on the opposite side of the particle (Fig. 3C).

We have also reconstructed models from AL and ST sheets stained with uranyl acetate. Although the arrays used were large and well ordered, the diffraction patterns of their micrographs extended only to 32 and 35 Å, respectively. The interaction of uranyl acetate with the particles may depend on the accessibility of the stain and therefore be somewhat irregular. Consequently, the reconstructed model showed less detail. For the ST sheets, the essential features (the concave shape, the tunnel, and the projecting arms) could be resolved. In the reconstruction obtained from AL and ST crystals stained with uranyl acetate, there were two regions (on one of the long arms and on the body of the particle) where uranyl acetate, acting as a positive stain, was incorporated into the particle. In these regions the rRNA may be concentrated or easily exposed to the stain.

Several models for the 50*S* ribosomal subunits from *E. coli* have been suggested on the basis of electron microscopical visualization and averaging of single particles (*10*). Our model is more similar to those having no flat surfaces and to those in which the projecting arms are arranged radially around one side of the particle. Moreover, our model can be positioned so that its projected view resembles the usual image seen when single particles are investigated by electron microscopy (Fig. 3E). In addition, a few filtered images of two-dimensional sheets tilted by certain angles show the same shape and include the characteristic features that have been visualized by electron microscopy of single particles (Fig. 4).

However, there are also major discrepancies in the nature of the gross structural features between our model and the others, discrepancies that probably stem from the basic differences between visualization of isolated particles and crystalline sheets. There are a few preferred orientations in which the isolated particles tend to lie on grids. As a result of the contact with the flat grids, their projected views are likely to be somewhat distorted and their surfaces may appear flat rather than curved. In contrast, particles within the crystalline sheets are held together by interparticle contacts. These contacts construct a network that may stabilize the conformation of the particles and decrease, or even eliminate, the influence of the flatness of the grids. Thus, the particles within ordered arrays provide a better starting point for reconstruction studies.

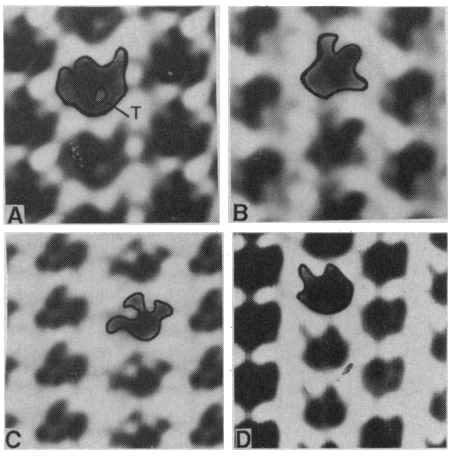

Fig. 4. Filtered images of electron micrographs in which the depicted view resembles that derived from electron microscopy of single particles. The particles are black and the background is white. (**A–C**) Filtered images of type (ST) sheets at 30°, 20°, and 35° tilt angles, respectively. The tunnel (T) can be seen. (**D**) Filtered image of type (AL) sheets at a tilt angle of 25°.

To understand why some of the features revealed in our studies have not been detected in previous investigations, we have reconstructed a model selecting from the entire set of diffraction data only the low-resolution (55 Å) terms. In the resulting model, in spite of the low resolution, the tunnel is clearly resolved. However, at this resolution the particle is almost spherical and shows only two thick and short arms instead of the elongated ones resolved in the 30 Å resolution studies (Fig. 5). Indications that at low resolution the particle may appear spherical could be detected in the low-resolution regions of several individual lattice lines (that is, $h;k = 1;-2$ or $2;-4$; Fig. 2) in which there is very little variation with tilting in amplitude or phase.

A recent model of whole ribosomes from chick embryos reconstructed at a resolution of 55 Å assigned a low-density region as a channel (*15*). However, the objects of these studies, 80*S* ribosomes, are significantly larger than ours and pack in larger unit cells (593 by 593 Å versus 152 by 350 Å). For these reasons and because of the relatively low resolution of the diffraction patterns of the two-dimensional sheets of the 80*S*, the details such as branching of the tunnel could not be revealed.

We have also reconstructed models from partial data sets (45 to 50% of the whole diffracting sphere at 30 Å) and observed that for the ST sheets these models show the main structural features: the tunnel, the concave shape, and the projecting arms. However, the partial data models appear as round objects with short arms, in contrast to the elongated oval shape of the entire particle obtained from the higher resolution set. In view of these results, it is not clear why the tunnel has not been detected in studies of negatively stained two-dimensional sheets of 50*S* subunits performed at a resolution of 40 Å (*16*).

There is a significant shortening of the long projecting arms in models reconstructed from crystals grown from alcohols. This may indicate that the arms that are positioned firmly in an environment of salts may flex when exposed to alcohols. Inherent flexibility of the long arms has also been

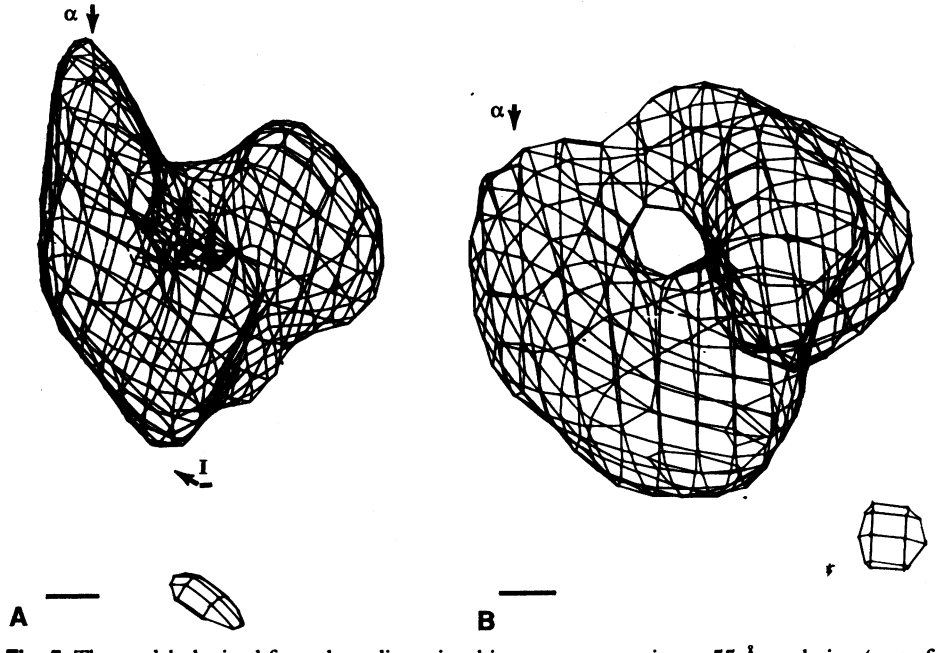

Fig. 5. The model obtained from three-dimensional image reconstruction at 55 Å resolution (part of the data used for Fig. 3A). (**A**) The view is from approximately the same direction as in Fig. 3B. Part of the second particle is shown and marked by I. (**B**) A view into the tunnel from the cleft. Bar length, 20 Å.

observed in reconstruction of rotated single particles (*17*).

The functional significance of the tunnel is still to be determined. However, it is possible that the tunnel could provide the path taken by the nascent polypeptide chain since (i) the tunnel originates at the projecting arms lying at the presumed site for protein biosynthesis (*10*) and it terminates on the other end of the particle, and (ii) it is of a diameter large enough to accommodate even the largest amino acids. Furthermore, this tunnel is long enough to accommodate and protect from proteolytic enzymes a peptide of about 40 amino acids in an extended conformation (*18–20*). Although the tunnel terminates at a location that may be compatible with that assigned by immune electron microscopy as the exit site for the growing polypeptide chain (*21*), it remains to be seen whether these two sites are identical.

Assignment of the known functional domains of the 50*S* ribosomal subunits to the various structural features of our model awaits further investigation. We hope to locate specific sites on a detailed model.

REFERENCES AND NOTES

1. H. G. Wittmann *et al.*, *FEBS Lett.* **146**, 217 (1982).
2. M. Shoham *et al.*, *ibid.* **208**, 321 (1986).
3. I. Makowski, F. Frolow, M. A. Saper, H. G. Wittmann, Y. Yonath, *J. Mol. Biol.* **193**, 819 (1987).
4. A. Yonath, H. D. Bartunik, K. S. Bartels, H. G. Wittmann, *ibid.* **177**, 201 (1984).
5. A. Yonath *et al.*, *ibid.* **187**, 633 (1986).
6. A. Yonath, M. A. Saper, H. G. Wittmann, in *Structure, Function and Genetics of Ribosomes*, B. Hardesty and G. Kramer, Eds. (Springer-Verlag, Heidelberg, 1986), pp. 112–127.
7. T. Arad, K. R. Leonard, H. G. Wittmann, A. Yonath, *EMBO J.* **3**, 127 (1984).
8. J. Piefke, T. Arad, H. S. Gewitz, A. Yonath, H. G. Wittmann, *FEBS Lett.* **209**, 104 (1986).
9. A. Yonath, *Trends Biochem. Sci.* **9**, 227 (1984).
10. H. G. Wittmann, *Annu. Rev. Biochem.* **52**, 35 (1983).
11. K. H. Nierhaus, K. Bordasch, H. E. Homann, *J. Mol. Biol.* **74**, 584 (1973).
12. B. W. Matthews, *ibid.* **33**, 491 (1968).
13. J. M. Hogle, *ibid.* **160**, 663 (1982).
14. T. Richmond, J. T. Finch, B. Rushton, D. Rhodes, A. Klug, *Nature (London)* **311**, 533 (1984).
15. R. A. Milligan and P. N. T. Unwin, *ibid.* **319**, 693 (1986).
16. M. W. Clark, K. Leonard, J. A. Lake, *Science* **216**, 999 (1982).
17. A. Verschoor, J. Frank, M. Boublik, *J. Ultrastruct. Res.* **92**, 180 (1985).
18. L. I. Malkin and A. Rich, *J. Mol. Biol.* **26**, 329 (1967).
19. G. Blobel and D. D. Sabatini, *J. Cell. Biol.* **45**, 130 (1970).
20. W. P. Smith, P. C. Tai, B. D. Davis, *Proc. Natl. Acad. Sci. U.S.A.* **75**, 5922 (1978).
21. C. Bernabeau and J. A. Lake, *ibid.* **79**, 3111 (1982).
22. L. A. Amos, R. Henderson, P. N. T. Unwin, *Progr. Biophys. Mol. Biol.* **39**, 183 (1982).
23. K. R. Leonard, P. Wingfield, T. Arad, H. Weiss, *J. Mol. Biol.* **149**, 259 (1981).
24. A. Jones, *J. Appl. Crystallogr.* **11**, 268 (1978).

25. We thank J. Piefke and T. Arad for conducting the electron microscopy experiments; J. L. Sussman for adapting the computer display programs; F. L. Hirshfeld for his interest and critical comments; B. Shaanan, H. Bosshard, M. A. Saper, and A. Levy for assistance with computer problems; and H. S. Gewitz, J. Müssig, B. Hennemann, and Y. Halfon for skillful technical assistance. Supported by NIH (GM34360), BMFT (05180 MPBO), and Minerva research grants.

12 September 1986; accepted 20 February 1987

Allelic Exclusion in Transgenic Mice That Express the Membrane Form of Immunoglobulin μ

MICHEL C. NUSSENZWEIG, ALBERT C. SHAW, ERIC SINN, DAVID B. DANNER, KEVIN L. HOLMES, HERBERT C. MORSE III, PHILIP LEDER

Antibody-producing cells display a special form of regulation whereby each cell produces immunoglobulin from only one of its two sets of antibody genes. This phenomenon, called allelic exclusion, is thought to be mediated by the product of one heavy chain allele restricting the expression of the other. Heavy chains are synthesized in two molecular forms, secreted and membrane bound. In order to determine whether it is specifically the membrane-bound form of the immunoglobulin M (IgM) heavy chain (μ) that mediates this regulation, transgenic mice were created that carry a human μ chain gene altered so that it can only direct the synthesis of the membrane-bound protein. The membrane-bound form of the human μ chain was made by most of the B cells in these animals as measured by assays of messenger RNA and surface immunoglobulins. Further, the many B cells that express the human gene do not express endogenous mouse IgM, and the few B cells that express endogenous mouse μ do not express the transgene. Thus, the membrane-bound form of the μ chain is sufficient to mediate allelic exclusion. In addition, the molecular structures recognized for this purpose are conserved between human and mouse systems.

REGULATION OF IMMUNOGLOBULIN gene expression involves genomic rearrangements at a minimum of two loci that bring regulatory and coding sequences into proximity (*1*). In addition, differential cleavage and polyadenylation of messenger RNA (mRNA) precursors generate either membrane or secreted forms of immunoglobulin heavy chains (*2–4*). Continued genomic rearrangements and splicing further generate a series of heavy chain classes (*5*). Although these changes often involve both parental sets of antibody genes, only one eventually directs the synthesis of a functional immunoglobulin in a given cell. This mechanism, allelic exclusion, is central to the process of clonal selection (*6*).

There is persuasive evidence that allelic exclusion at the light chain loci is mediated by intact immunoglobulin molecules (*7, 8*). In addition, experiments with transgenic mice suggest that expression of endogenous heavy chain alleles can be influenced by an introduced murine μ chain transgene (*9–11*). Evidence thus far indicates that the human γ-1 gene (*12*) and a version of the mouse μ gene that gives rise to a secreted form of the mouse μ chain (*11*) do not mediate this process. Since immunoglobulin M (IgM) heavy chains are produced in two forms, membrane-bound and secreted, it is reasonable to suggest that such a regulatory signal is mediated by a membrane-bound molecule (*11*) because the secreted form is sequestered in the vacuolar system. To test this theory we created transgenic mice (*13*) that carry a rearranged human μ gene altered to delete the cleavage and polyadenylation signals necessary to synthesize the secreted form of the μ heavy chain (*3*). The mutant gene (Fig. 1A) is capable of producing only the membrane-bound form of the molecule in transfected tissue culture cells.

Expression of the human transgene and the endogenous mouse μ mRNAs was assessed by ribonuclease protection experiments with probes that are species specific and can distinguish between the mRNAs encoding membrane-bound and secreted forms of the μ chain (Fig. 1). Spleen cells derived from two transgenic lines, TG SA and TG SD, were used for this analysis. The two lines expressed the membrane-bound form of the human gene but differed in the amount of expression (Fig. 1B). Densitometric analysis of data from these experiments shows that spleen cells from mice of the TG SA line produce 25 to 35

M. C. Nussenzweig, A. C. Shaw, E. Sinn, P. Leder, Department of Genetics, Harvard Medical School, and Howard Hughes Medical Institute, Boston, MA 02115.
D. B. Danner, Laboratory of Molecular Genetics, National Institute on Aging, Baltimore, MD 21224.
K. L. Holmes and H. C. Morse III, Laboratory of Immunopathology, National Institute of Allergy and Infectious Diseases, National Institutes of Health, Bethesda, MD 20892.